Multiscale modeling of magnetospheric reconnection

M. M. Kuznetsova,[1] M. Hesse,[1] L. Rastätter,[1] A. Taktakishvili,[1] G. Toth,[2] D. L. De Zeeuw,[2] A. Ridley,[2] and T. I. Gombosi[2]

Received 1 February 2007; revised 3 June 2007; accepted 10 July 2007; published 12 October 2007.

[1] In our efforts to bridge the gap between small-scale kinetic modeling and global simulations, we introduced an approach that allows to quantify the interaction between large-scale global magnetospheric dynamics and microphysical processes in diffusion regions near reconnection sites. We use the global MHD code BATS-R-US and replace an ad hoc anomalous resistivity often employed by global MHD models with a physically motivated dissipation model. The primary kinetic mechanism controlling the dissipation in the diffusion region in the vicinity of the reconnection site is incorporated into the MHD description in terms of nongyrotropic corrections to the induction equation. We developed an algorithm to search for reconnection sites in north-south symmetric magnetotail. Spatial scales of the diffusion region and magnitude of the reconnection electric field are calculated consistently using local MHD plasma and field parameters. The locations of the reconnection sites are constantly updated during the simulations. To clarify the role of nongyrotropic effects in the diffusion region on the global magnetospheric dynamics, we perform simulations with steady southward interplanetary magnetic field driving of the magnetosphere. Ideal MHD simulations with magnetic reconnection supported by numerical resistivity often produce quasi-steady configuration with almost stationary near-Earth neutral line (NENL). Simulations with nongyrotropic corrections demonstrate dynamic quasi-periodic response to the steady driving conditions. Fast magnetotail reconnection supported by nongyrotropic effects results in tailward retreat of the reconnection site with average speed of the order of 100 km/s followed by a formation of a new NENL in the near-Earth thin current sheet. This approach allowed to model for the first time loading/unloading cycle frequently observed during extended periods of steady low-mach-number solar wind with southward interplanetary magnetic field.

Citation: Kuznetsova, M. M., M. Hesse, L. Rastätter, A. Taktakishvili, G. Toth, D. L. De Zeeuw, A. Ridley, and T. I. Gombosi (2007), Multiscale modeling of magnetospheric reconnection, *J. Geophys. Res.*, *112*, A10210, doi:10.1029/2007JA012316.

1. Introduction

[2] One of the major challenges in modeling the magnetospheric magnetic reconnection is to quantify the interaction between large-scale global magnetospheric dynamics and microphysical processes in diffusion regions near reconnection sites. Magnetospheric modelers are actively debating to what degree the microphysical processes on kinetic scales affect the global evolution and how important it is to substitute numerical dissipation and/or ad hoc anomalous resistivity by a physically motivated model of dissipation.

[3] Recent advances in small-scale kinetic modeling of magnetic reconnection significantly improved our understanding of physical mechanisms controlling the dissipation in the vicinity of the reconnection site in collisionless plasma [e.g., *Hesse et al.*, 2005; *Hesse*, 2006; *Hoshino et al.*, 2001; *Pritchett*, 2001b, 2005; *Pritchett and Coroniti*, 2004; *Drake et al.*, 2003; *Karimabadi et al.*, 2004; *Daughton et al.*, 2006; *Shay et al.*, 2004; *Zeiler et al.*, 2002; *Rogers et al.*, 2001, 2003]. However the progress in studies in small-scale geometries has not yet been applied to large-scale simulations. Global magnetosphere MHD simulations usually include nonideal processes in terms of numerical dissipation and/or ad hoc anomalous resistivity η [*Powell et al.*, 1999; *Raeder et al.*, 2001; *Ashour-Abdalla et al.*, 1999; *Wiltberger et al.*, 2000; *Raeder et al.*, 2001; *Slinker et al.*, 2001; *Tóth et al.*, 2005]. In such models the magnitude of resistivity and spatial scales of resistivity localization are chosen without any theoretical justification. Resistivity levels used in global MHD simulations of magnetotail dynamics are many orders of magnitude above the estimated anomalous resistivity values associated with current-driven microinstabilities such as, e.g., the lower-hybrid drift instability [*Huba et al.*, 1977; *Sotnikov et al.*, 1981; *Kuznetsova and Nikutowski*, 1994], or tearing instability destabilized by quasi-adiabatic electrons [*Büchner and Zelenyi*, 1988; *Büchner and Otto*, 1995]. The theoretical approach based on linear and quasi-linear analysis aimed to study the

[1]Space Weather Laboratory, NASA Goddard Space Flight Center, Greenbelt, Maryland, USA.
[2]Center for Space Environment Modeling, University of Michigan, Ann Arbor, Michigan, USA.

0148-0227/07/2007JA012316

stability of equilibrium magnetic configurations is not applicable at the reconnection site after the reconnection onset. For example, in two-dimensional medium-scale MHD simulations *Büchner and Otto* [1995] utilized the values of anomalous resitivity estimated for initial profile of the normal magnetic field component in the tail-like quasi-equlibrium magnetic configuration. The resistivity was kept fixed in time, while the magnetic configuration significantly changed after the reconnection onset.

[4] There is a growing number of observational evidences of dynamic quasi-periodical magnetosphere response to continuously southward interplanetary magnetic field (IMF) [*Borovsky et al.*, 1993, 2004; *Huang et al.*, 2005; J. E. Borovsky et al., The solar-wind driving of periodic substorms and global stormtime sawtooth oscillations: What determines the periodicity, submitted to *Annales Geophysicae*, 2007, hereinafter referred to as Borovsky et al., submitted manuscript, 2007]. However, ideal global MHD simulations with magnetic reconnection supported by numerical resistivity driven by steady southward IMF often produce only quasi-steady configurations with almost stationary near-Earth neutral line (NENL) [*Borovsky et al.*, 2004]. This discrepancy can be explained by the assumption that global MHD simulations significantly underestimate the reconnection rate in the magnetotail during substorm expansion phase. Indeed, comparative studies of magnetic reconnection in small-scale geometries demonstrated that traditional resistive MHD did not produce the fast reconnection rates observed in kinetic simulations [*Birn et al.*, 2001; *Birn and Hesse*, 2001; *Otto*, 2001; *Hesse et al.*, 2001; *Pritchett*, 2001a; *Birn et al.*, 2005].

[5] The major approximation of the traditional MHD approach is an isotropic fluid assumption, with zero off-diagonal pressure tensor components. The approximation, however, becomes invalid in the diffusion region around the reconnection site where ions become unmagnetized and experience nongyrotropic behavior. At the same time, presently there is little doubt that kinetic effects play a significant role in collisionless magnetic reconnection and the particle distribution functions in diffusion region are essentially nongyrotropic. Deviation from gyrotropy in particle distribution function caused by kinetic effects manifests itself in nongyrotropic pressure tensor with nonzero off-diagonal components.

[6] The purpose of this study is to develop and test an approach that allows us to replace the traditional model depending on ad hoc anomalous resistivity in global MHD simulations, with a physically motivated model of dissipation. We will take advantage of recent progress in small-scale kinetic studies and incorporate the most essential physics that controls fast reconnection rates to the magnetic induction equation (Faraday's Law). Specifically, in the diffusion region around the reconnection site, where isotropic fluid MHD approximation is not applicable, we will treat the ions as nongyrotropic fluid. Spatial scales of the diffusion region and magnitude of the non-MHD corrections will be calculated using local MHD plasma and field parameters without introduction of any ad hoc factors. We will investigate how the new dissipation model affects the overall dynamics of reconnection-related changes in magnetosphere.

[7] The paper is structured as follows. In section 2 we present a brief overview of the MHD approach with nongyrotropic corrections. In section 3 we describe the global MHD simulation setup. Results of global MHD simulations with nongyrotropic corrections are presented in section 4. The summary and conclusions are in section 5.

2. Nongyrotropic Corrections to the MHD Approach

[8] For a broad range of physical parameters, the primary mechanism controlling the dissipation in the vicinity of the reconnection site in collisionless magnetospheric plasma is associated with nongyrotropic pressure effects with spatial scales comparable to the particle Larmor radius [*Hesse and Winske*, 1998; *Hesse et al.*, 1999, 2001, 2004, 2005; *Hesse*, 2006; *Kuznetsova et al.*, 1998, 2000, 2001; *Ricci et al.*, 2002, 2004; *Pritchett*, 2001a; *Yin et al.*, 2001; *Yin and Winske*, 2003].

[9] In collisionless plasma the Y component of the Ohm's law (electron momentum equation) provides expression for all contributions to the electric field responsible for violation of the frozen flux constraint in the diffusion region

$$E_y = -[\mathbf{v}_i \times \mathbf{B}]_y + \frac{1}{ne}[\mathbf{J} \times \mathbf{B}]_y - \frac{1}{ne}\left(\frac{\partial P_{exy}}{\partial x} + \frac{\partial P_{ezy}}{\partial z}\right) - \frac{m_e}{e}\frac{dv_{ey}}{dt} \tag{1}$$

[10] Here the Y axis is pointed along the main current direction at the reconnection site ($X = 0$, $Z = 0$). The Hall current is in the $X - Z$ plane perpendicular to Y. The Hall term $[\mathbf{J} \times \mathbf{B}]_y$ is equal to zero exactly at the reconnection site. The dominant term in Y component of the the Ohm's law in the immediate vicinity of the reconnection site ($X = 0$, $Z = 0$) is the contribution to the electric field E_y^{ng} from the off-diagonal components of electron nongyrotropic pressure tensor:

$$E_0^{\mathrm{ng}} = E_y^{\mathrm{ng}}\Big|_{x,z=0} \approx -\frac{1}{ne}\left(\frac{\partial P_{exy}}{\partial x} + \frac{\partial P_{ezy}}{\partial z}\right)_{x,z=0} \approx \frac{1}{e}\sqrt{2m_eT_e}\frac{\partial v_{ex}}{\partial x}\Big|_{x,z=0} \tag{2}$$

[11] In equations (1) and (2) n, v_{ex}, v_{ey},e, m_e, T_e denote number density, X and Y components of the electron bulk flow velocity, charge, electron mass and electron temperature, respectively. Analytical estimates given in (2) for the gradients of the off-diagonal pressure tensor components P_{exy}, P_{ezy} for the case of zero B_y magnetic field component along the main current direction Y are derived from the evolution equation of full electron pressure tensor $\underline{\mathbf{P}}_e$ (second moment of Vlasov equation), neglecting the divergence of the generalized heat flux contribution [*Hesse et al.*, 1999; *Kuznetsova et al.*, 2000, 2001].

[12] Kinetic simulations demonstrated that the reconnection rate is practically independent of the electron mass and temperature [*Hesse et al.*, 1999, 2001; *Pritchett*, 2001a; *Bessho and Bhattacharjee*, 2005]. Taking advantage of these results, *Kuznetsova et al.* [2000] expressed nongyrotropic pressure contribution to the electric field at the reconnection site ($x = 0$, $z = 0$) through single-fluid plasma

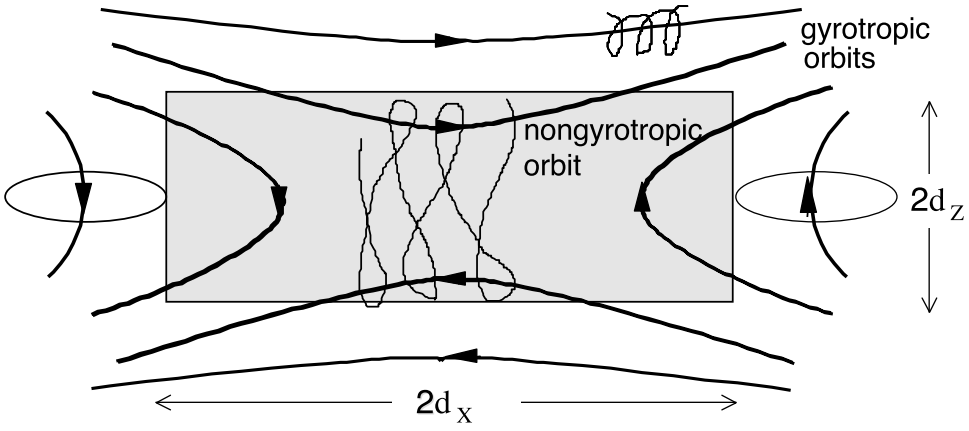

Figure 1. Schematic structure of the diffusion region near the reconnection site in collisionless plasmas. Y axis is along the current direction at the magnetically neutral point. Z axis is normal to the current sheet. X is axis along the outflow direction. Inside the grey area ions are unmagnetized. At the edge of the diffusion region ion Larmor radius is equal to the distance to the neutral point. Outside of the grey area plasma is magnetized.

parameters (temperature T and bulk flow velocity v_x), by replacing m_e, T_e and v_{ex} in expression (2) with ion mass, temperature and bulk flow velocity m_i, $T_i = T$, $v_{ix} = v_x$.

$$E_0^{\mathrm{ng}} \approx \frac{1}{e}\sqrt{2m_iT}\left.\frac{\partial v_x}{\partial x}\right|_{x,z=0} \tag{3}$$

[13] Reconnection electric field estimated from the simple formula (3) is in excellent agreement with an actual reconnection electric field taken from kinetic simulations [*Kuznetsova et al.*, 2001, Plate 2]. Analytical estimates for the time evolution of the reconnected flux derived from (3) and MHD equation of motion [*Kuznetsova et al.*, 2000, Figure 6] perfectly match the results of comprehensive hybrid and particle simulations [*Kuznetsova et al.*, 2000, 2001; *Hesse et al.*, 2001].

[14] The major approximation of the traditional MHD approach is an isotropic fluid assumption, which becomes invalid in the diffusion region $2d_x \times 2d_z$ around the reconnection site (Figure 1), where ions become unmagnetized and experience nongyrotropic behavior. Here the Y axis is pointed along the main current direction at the reconnection site ($x = 0$, $z = 0$), the Z axis is normal to the current sheet, and the X axis is along the outflow direction. Outside of the diffusion region $|x| > d_x$, $|z| > d_z$ ions and electrons are magnetized and move together, the single-fluid isotropic MHD approach is applicable, and the frozen magnetic flux constraint $\mathbf{E} + \mathbf{v} \times \mathbf{B} = 0$ is valid.

[15] In the vicinity of the reconnection site magnetic field components B_z and B_x can be expanded in Taylor series: $B_z(x, 0) \approx B'_z x$, $B_x(0, z) \approx B'_x z$, where $B'_z = (\partial B_z/\partial x)_{x,z=0}$, $B'_x = (\partial B_x/\partial z)_{x,z=0}$. The spatial scales of the diffusion region (Figure 1) can be estimated from the gyrotropic orbit threshold condition, where the ion gyroradius r_i becomes equal to the distance to the reconnection site, $r_i(d_x, 0) = d_x$, $r_i(0, d_z) = d_z$.

$$d_x = \left(2m_iT/e^2B_z'^2\right)^{1/4}, \quad d_z = \left(2m_iT/e^2B_x'^2\right)^{1/4} \tag{4}$$

[16] The estimate in (4) is a typical dimension of the ion meandering orbits in magnetic field reversal. At the outflow edges of the diffusion region $|x| = d_x$, $z = 0$, where the frozen flux approximation is still valid, the Y component of the electric field is equal to the convection electric field

$$E_y(d_x, 0) = v_x(d_x, 0)B_z(d_x, 0) \approx v'_x B'_z d_x^2 \tag{5}$$

where $v'_x = (\partial v_x/\partial x)_{x,z=0}$.

[17] Expression (5) describes the rate of convection of reconnected magnetic flux out of the diffusion region. From the continuity consideration the rate of convection of reconnected flux out of the diffusion region should match the rate of production of the reconnected flux inside the diffusion region, which is equal to the reconnection rate E_y^{rec}. Substituting the expression for d_x (4) into (5), one can find the simple estimate for the reconnection electric field E_y^{rec} that matches the expression (3) derived from the evolution equation of the full particle pressure tensor. Thus the reconnection electric field can be estimated as the convection electric field $\mathbf{E} = -\mathbf{v} \times \mathbf{B}$ at the outflow boundary of the diffusion region.

[18] To maintain quasi-neutrality the Y component of the Ohm's law (1) should match the electric filed in the first moment of the Vlasov equation for ions

$$E_y = -[\mathbf{v}_i \times \mathbf{B}]_y + \frac{1}{ne}\left(\frac{\partial P_{ixy}}{\partial x} + \frac{\partial P_{izy}}{\partial z}\right) + \frac{m_i}{e}\frac{dv_{iy}}{dt} \tag{6}$$

[19] The nongyrotropic pressure term in (6), which scales as $(m_iV/e)(V_{Ti}/d_x)$, is larger than the ion inertia term, which scales as $(m_iV/e\tau)$, as long as the time required for the thermal ion to cross the diffusion region d_x/V_{Ti} is faster than the characteristic time τ of the system evolution: $\tau > d_x/V_{Ti}$.

[20] From equations (1) and (6) it is seen that inside the diffusion region the ion nongyrotropic pressure term matches the Hall term and electron nongyrotropic pressure contributions to the reconnection electric field. Therefore nonideal effects localized in the diffusion region $|x| < d_x$, $|z| < d_z$ can be incorporated into the new MHD model in terms

of nongyrotropic pressure corrections E^{ng} to the electric field in the Faraday's law

$$\frac{\partial \mathbf{B}}{\partial t} = -\nabla \times \left(-\mathbf{v} \times \mathbf{B} + E^{ng}\mathbf{e}_y\right) \quad (7)$$

$$E^{ng} = \frac{1}{ne}\left(\frac{\partial P_{ixy}}{\partial x} + \frac{\partial P_{izy}}{\partial z}\right) \quad (8)$$

$$E^{ng}|_{x,z=0} = E_0^{ng}, \quad E^{ng}|_{|x|>d_x,|z|>d_z} \rightarrow 0 \quad (9)$$

[21] Here $\mathbf{e}_y$ is a unity vector along the current direction at the reconnection site, E_0^{ng} is given in (3).

[22] The arguments and estimates presented above lead us to a simple technique of multiscale modeling of magnetospheric reconnection aiming to identify areas where the MHD approximation does not work and modify traditional MHD in these areas by adding kinetic corrections to the electric field. The technique can roughly be outlined as a three-step procedure:

[23] 1. Find the locations of the reconnection sites ($x_0(y)$, $z_0(y)$), ..., ($x_m(y)$, $z_m(y)$), ... $m = 0, 1, \ldots$;

[24] 2. Calculate magnitudes of reconnection electric field supported by nongyrotropic effects E_0^{ng} and spatial scales of diffusion regions d_x and d_z for each reconnection site ($x_m(y)$, $z_m(y)$);

$$E_0^{ng} = \frac{m_i}{e}\sqrt{\frac{2P}{\varrho}}v'_x \quad (10)$$

$$d_x^2 = \frac{m_i}{eB'_z}\sqrt{\frac{2P}{\varrho}}, \quad d_z^2 = \frac{m_i}{eB'_x}\sqrt{\frac{2P}{\varrho}} \quad (11)$$

[25] Here P, ρ, $v'_x = \partial v_x/\partial x$ are pressure, mass density, and gradient of the bulk flow velocity at the reconnection site, m_i is the ion mass. In normalized form used in MHD simulations expressions (10) and (11) take the following form

$$\overline{E}_0^{ng} = \alpha\sqrt{2\frac{\overline{P}}{\overline{\varrho}}}\overline{v}'_x, \quad \alpha = \frac{r_{i0}}{R_E} \quad (12)$$

$$\overline{d}_x = \left(2\overline{P}\alpha^2/\overline{\varrho}\overline{B}'^2_z\right)^{1/4}, \quad \overline{d}_z = \left(2\overline{P}\alpha^2/\overline{\varrho}\overline{B}'^2_x\right)^{1/4}, \quad (13)$$

[26] Here $\overline{E}_0^{ng} = \overline{E}_0^{ng}/E_0$, $\overline{d}_x = d_x/R_E$, $\overline{d}_z = d_z/R_E$, R_E is the Earth's radius, $E_0 = V_0 B_0$ is characteristic value of electric field. Parameters $r_{i0} = \sqrt{2P_0/\rho_0}/\Omega_{i0}$ and $\Omega_{i0} = eB_0/m_i$ are ion Larmor radius and gyrofrequency for characteristic values of pressure P_0, mass density ρ_0, and magnetic field B_0, used to perform normalization of MHD variables and equations.

[27] 3. Add nongyrotropic corrections to the electric field spatially localized in diffusion regions

$$E_y^{ng} = E_0^{ng} \cdot f((x - x_m)/d_x, (z - z_m)/d_z), \quad (14)$$

where $f((x - x_m)/d_x, (z - z_m)/d_z)$ is an arbitrary cutoff function with gradient scales d_x and d_z, ($f/(\partial f/\partial x) = d_x$, $f/(\partial f/\partial z) = d_z$). The cutoff function f is equal to unity at the reconnection site $x = x_k$, $z = z_k$ and tends to zero at the edges of the diffusion region.

[28] The MHD model with nongyrotropic corrections to the electric field described above has been tested for GEM Challenge settings [*Birn et al.*, 2001] in the recently submitted paper by M. M. Kuznetsova et al. (MHD modeling of fast magnetic reconnection, submitted to Physics of Plasmas, 2007, hereinafter referred to as Kuznetsova et al., submitted manuscript, 2007). Reconnection rates simulated in the new MHD model match the fast reconnection rates observed in kinetic simulations for a similar setup. Current density and magnetic field patterns in the vicinity of the reconnection site are also consistent with those observed in kinetic simulations. The success of this comparative study encouraged us to implement the technique to global MHD simulations of magnetotail reconnection.

3. Simulation Setup

[29] We employed the global MHD code BATS-R-US developed at Center for Space Environment Modeling (CSEM) at the University of Michigan. BATS-R-US is Global Magnetosphere component of the Space Weather Modeling Framework (SWMF) designed to model the space environment for various space physics applications. SWMF contains nine models that cover the various regions between the Sun and Earth. Simulations presented in this paper utilize only Global Magnetosphere (GM) and Ionosphere Electrodynamics (IE) modeles. An in-depth discussion of BATS-R-US and SWMF can be found in the work of *Powell et al.* [1999], *Gombosi et al.* [2002], and *Tóth et al.* [2005].

[30] The global MHD code BATSRUS solves the ideal MHD equations (conservation of mass, momentum, and energy equations and a Faraday's law) with a finite volume discretization. A full set of equations in conservative form and the numerical method can be found in the works of *Powell et al.* [1999] and *Gombosi et al.* [2004]. BATS-R-US is designed using Fortran 90 and Message Passing Interface (MPI) standards. BATS-R-US implements a block-based domain-decomposition technique. The simulation grid is composed of many self-similar three-dimensional rectangular blocks arranged in varying degrees of spatial refinement levels. To optimize the load-balance the simulation blocks are evenly distributed between processors of the parallel computer system. Blocks communicate with neighbors through layers of "ghost" cells. The adaptive block-based hierarchical data structure allows one to increase resolution where and when it is needed. The BATS-R-US adaptive grid structure makes it possible to perform global simulations with spatial resolution near reconnection sites comparable to ion kinetic scales. Our calculations utilize a grid composed of self-similar blocks consisting of $6 \times 6 \times 6$ cells each with additional double layers of ghost cells at each edge of the block. The simulation box size in GSM coordinates is $-351\ R_E < X < 33\ R_E$, $|Y| < 96\ R_E$, $|z| < 96\ R_E$. The simulation grid with about 20,000,000 grid cells provides resolution of 1/8 R_E within $3R_E$ of the equatorial plane in significant portion of the magnetosphere ($-90\ R_E < X <$

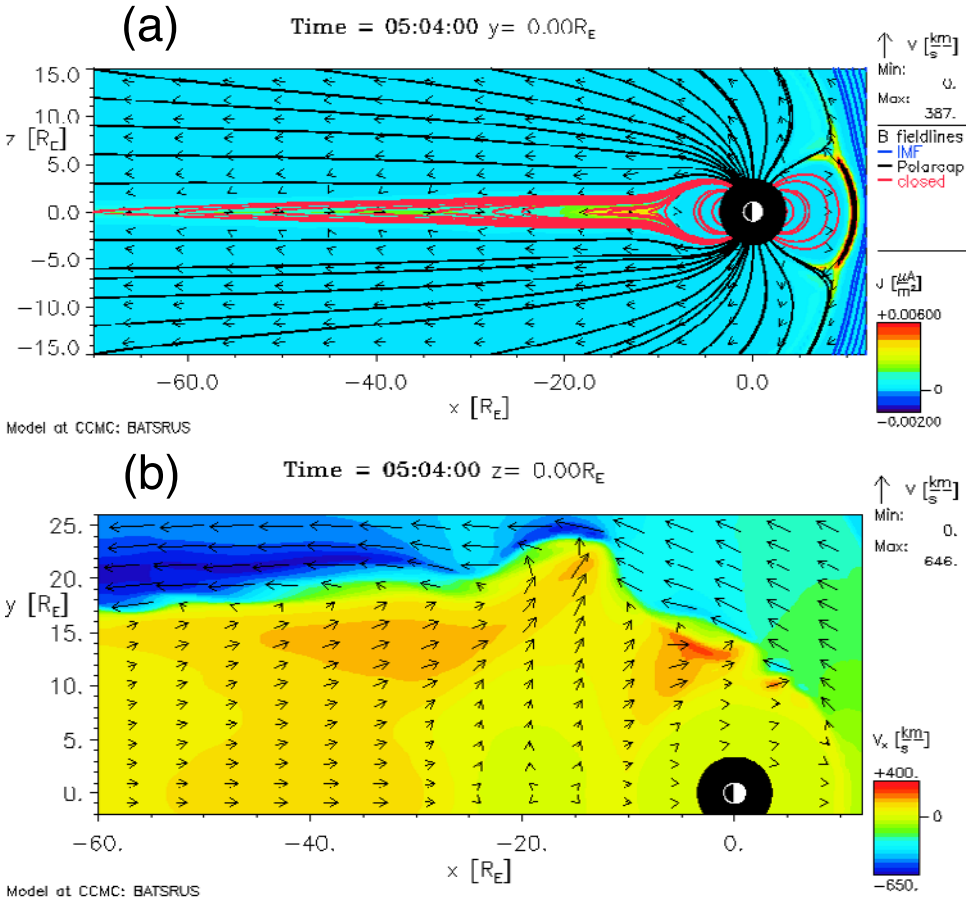

Figure 2. Magnetosphere 1 min prior to reconnection onset in the magnetotail. (a) Color-coded current density distribution at $Y = 0$ plane. Arrows correspond to velocity vectors. Blue lines are interplanetary field lines with both open ends, red lines are closed field lines connecting northern and southern polar regions, and black lines are semiopen filed lines connections polar regions to interplanetary magnetic field (IMF). (b) Color-coded V_x component of the flow velocity vector at the equatorial plane $Z = 0$.

12 R_E, $|Y| < 26$ R_E, $|Z| < 3$ R_E), which cover the dayside magnetopause, low-latitude boundary layer, and majority of reconnection sites in the magnetotail.

[31] The near-Earth boundary of the GM domain is located at 2.5 R_E from the center of the Earth. Near-Earth boundary conditions are determined by the IE module. The IE module is a two-dimensional electrostatic potential solver that obtains the field-aligned currents from GM and delivers convection velocity at the boundary back to GM [*Goodman*, 1995, 1996; *Amm*, 1996; *Soyka et al.*, 1997]. For simulation of real events the height-integrated conductance model used by IE includes effects of EUV, starlight and particle precipitation [*Ridley et al.*, 2004]. For our calculations we use constant Pedersen (equal to 5 mhos) and vanishing Hall conductivities.

[32] For the inflow boundary conditions at $X = 33$ R_E we choose low-mach-number ''sawtooth-solar-wind'' [*Borovsky*, 2004] with parameters close to average solar wind conditions during 18 April 2002 sawtooth event: $N = 2$ cm^{-3}, $T = 200{,}000$ K, $V_x = -400$ km/s, $V_y = V_z = 0$, $|B_z| = 10$ nT. The IMF is aligned with the Z-axis ($B_x = 0$, $B_y = 0$) and the Earth's magnetic dipole tilt is set to zero. These symmetric settings allow us to constrain magnetotail reconnection to close vicinity of the GSM equatorial plane $Z = 0$ in order to simplify the search for reconnection sites.

[33] The simulations were initiated with southward IMF ($B_z = -10$ nT). After 1 hour the IMF was turned northward ($B_z = 10$ nT) and kept northward for another 3 hours. At time stamp 4:00 the IMF was turned southward again and then kept southward ($B_z = -10$ nT) for another 5 hours up to the end of the simulation at time stamp 9:00.

[34] The time interval of interest started at time stamp 4:00 when the IMF was turned southward after a long period of northward orientation. The southward IMF turning causes a gradual magnetotail stretching accompanied by a current sheet thinning in the near-Earth region. The reconnection onset in the thin current sheet occurred in about an hour after the southward IMF turning.

[35] The search for magnetotail reconnection sites is activated at time stamp 5:05, immediately after the reconnection onset. The reconnection sites are searched near the equatorial plane $Z = 0$ within the area -80 $R_E < X < 3$ R_E, $|Y| < 18$ R_E, located inside the magnetotail within uniformly resolved spatial domain.

[36] To search for reconnection sites we took advantage of BATS-R-US block-based structure and parallel architec-

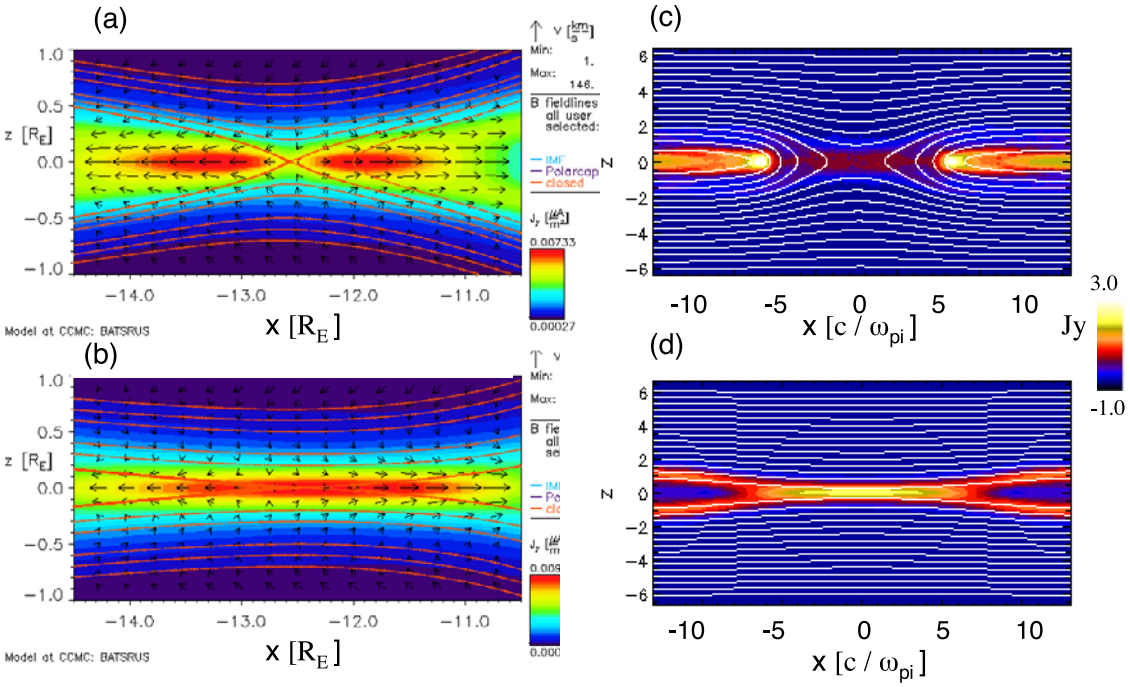

Figure 3. Magnetic field (contour lines) and Y component of the current density distributions (color-coded) in the vicinity of the reconnection site four minutes after reconnection onset for various simulations: (a) Global MHD with kinetic corrections. (b) Global MHD simulations with numerical resistivity only. (c) Kinetic simulations for GEM Reconnection Challenge geometry. (d) Resistive MHD for GEM Reconnection Challenge geometry. Current density for GEM Challenge simulations are normalized on $B_0\omega_{pi}/c\mu_0$.

ture. Arrays of X, Z locations of reconnection sites $X_m(n)$, $Z_m(n)$ are searched separately in each $Y = Y(n)$ plane ($|Y| < 18R_E$) well inside the area of uniform spatial resolution $\Delta x = \Delta y = \Delta z = 1/8\ R_E$. Magnetotail reconnection sites are searched within one block of the equatorial plane (i.e., $|Z| < \Delta z \times 6 = 0.75\ R_E$), which is justified for the symmetric setting used in present simulations. Index n ($n = 1,\ldots, N$; $N = 36/\Delta y + 1$) indicates the Y location of the reconnection site within $|Y| < 18R_E$: $Y(n) = -18\ R_E + \Delta y \times (n - 1)$. Index m corresponds to the location of the reconnection site in respect to the distance to the Earth: $m = 0$ corresponds to the closest to the Earth reconnection site in $Y = Y(n)$ plane, $m = 1$ corresponds to the next reconnection site $X_1(n)$ tailward of $X_0(n)$, and so on. The search for reconnection sites is performed in parallel in each block. Each block with $6 \times 6 \times 6$ cells (i, j, k) first checks for its location: whether it intersects the equatorial plane $Z = 0$ and $Y = Y(n)$ plane and whether it is located inside the $-80\ R_E < X < 3R_E$ interval. If the check is successful the index j_n where $y(i, j_n, k) = Y(n)$ is identified. Then the block checks for the presence of the reconnection site, that is, whether at one of its (i, j_n, k) cells both B_z and B_x magnetic field component change sign ($B_z(i - 1, j_n, k) < 0$, $B_z(i + 1, j_n, k) > 0$, $B_x(i, j_n, k - 1) < 0$, $B_x(i, j_n, k + 1) > 0$). The blocks then exchange information using MPI library calls to sort all found reconnection sites depending on their distances to the Earth and assign values to the $X_m(n)$, $Z_m(n)$ arrays. The spatial scales of the (m, n) diffusion region $d_x(m, n)$, $d_z(m, n)$ (10) and the magnitude of the reconnection electric filed $E_0^{ng}(m, n)$ (11) are calculated using MHD variables and their gradients at the grid cell where the corresponding reconnection site (m, n) is found. To localize the nongyrotropic correction to the difffusion region, we utilize the same inverse hyperbolic smooth cutoff function

$$f = \cosh^{-1}\left(\frac{2(x - x_m)}{d_x}\right)\cosh^{-1}\left(\frac{2(z - z_m)}{d_z}\right), \qquad (15)$$

that was employed by Kuznetsova et al. (submitted manuscript, 2007), where an excellent match with kinetic simulation results was produced.

[37] The nongyrotropic contribution to the electric field at each grid point (i, j, k) within $|y| < 18R_E$ takes the following form:

$$E_y^{ng}(i,j,k) = \sum_m E_0^{ng}(m,n)\cosh^{-1}\cdot\left(\frac{x(i,j,k) - x_m(n)}{d_x(m,n)/2}\right) \cdot \cosh^{-1}\cdot\left(\frac{z(i,j,k) - z_m(n)}{d_z(m,n)/2}\right), \qquad (16)$$

where $n = 1 + (y(i, j, k) + 18)/\Delta y$. The nongyrotropic corrections (16) are added to the source term of the Faraday's law (7). The curl of $E^{ng}(i, j, k)\mathbf{e}_y$ in (7) is taken analytically. Other MHD equations are not modified. Locations of reconnection sites, spatial scales of the diffusion region and the magnitude of the reconnection

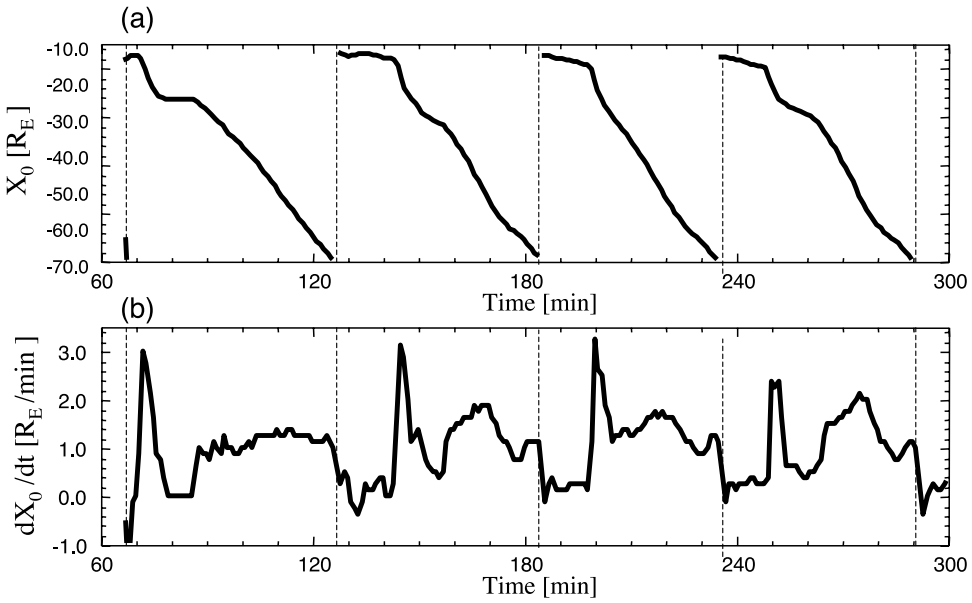

Figure 4. Tailward retreat of reconnection site. (a) Position of the closest to the Earth reconnection site X_0 for $Y = 0$. (b) Speed of reconnection site retreat. Time is measured in minutes past after the southward turning at time stamp 04:00.

electric filed for each reconnection site, are updated at each time step.

4. Simulation Results

[38] Figure 2 shows the magnetosphere configuration one minute prior to magnetotail reconnection onset. Colors display current density distribution in the meridional $Y = 0$ plane (Figure 2a) and value of V_x component of bulk flow velocity in the equatorial $Z = 0$ plane (Figure 2b). Arrows correspond to velocity vectors, while colored lines are magnetic field lines. In response to southward IMF turning, the magnetosphere forms a stretched tail with thin current sheet embedded between $-20R_E$ and $-10R_E$ (Figure 2a). The magnetotail stretching is accompanied with generation of large amplitude vortices at magnetospheric flanks. Generation of vortices is caused by Kelvin-Helmholtz instability excited in a velocity shear boundary layer in the plane perpendicular to the anti-parallel magnetic field (Figure 2b). Simulation with sharp velocity gradients that are necessary for the fast growth of surface waves becomes possible due to high spatial resolution at the magnetospheric flanks (up to 1/8 R_E).

[39] Effects of nongyrotropic corrections become clearly evident in just a few minutes after the reconnection onset. They are illustrated at side-by-side plots of magnetic field and current density distribution in the vicinity of the reconnection site for four different models (Figure 3). Figures 3a and 3b are "zoomed-in" magnetic field (contour lines) and current density distributions (color-coded) for global simulations with nongyrotropic corrections (Figure 3a) and global simulations with numerical resistivity only (Figure 3b). Other plots at Figures 3 show the results of small scale two-dimensional kinetic (Figure 3c) and resistive MHD (Figure 3d) simulations for GEM Reconnection Challenge settings [*Kuznetsova et al.*, 2000, 2001; Kuznetsova et al., submitted manuscript, 2007]. The dimensions of the "zoomed-in" area, 5 $R_E \times 2$ R_E around the reconnection site $X = -12.5$ R_E, $Y = 0$, $Z = 0$ shown at Figure 3a and 3b are chosen to approximately match the size of the simulations box used in the GEM Reconnection Challenge (Figures 3c and 3d). Here we took into account that spatial scales in the GEM Reconnection Challenge simulations (Figures 3c and 3d) are normalized to the ion skin depth c/ω_{pi}. The value of the ion skin depth, equal to 1/6 R_E, is estimated using average value of plasma density in the central plasma sheet in global simulations. Magnetic field and current density patterns for global simulations with nongyrotropic corrections (Figure 3a) and for small-scale kinetic simulations (Figure 3c) exhibit striking resemblance in the vicinity of the reconnection site. In particular, in both models the areas of increased current density are ejected away from the X-point, and the current density exhibits a saddle-point at the reconnection site. The diffusion region length is relatively small, which is a characteristic feature of fast reconnection. On the contrary, global MHD simulations with numerical resistivity, that disregard kinetic nongyrotropic effects (Figure 3b), and traditional small-scale resistive MHD simulations (Figure 3d), are both characterized by a stretched diffusion region with increased current density and a slow reconnection rate.

[40] The location of the reconnection site X_0 closest to the Earth for $Y = 0$ and the speed of its motion along the tail dX_0/dt is illustrated at Figures 4a and 4b. Time is counted in minutes after the southward turning at time stamp 04:00. Reconnection is initiated between -15 R_E and -10 R_E and then retreats tailward to -20 R_E. For simulations with reconnection supported by numerical resistivity only, the reconnection site settles at about -20 R_E and stays there afterward. Almost steady-state magnetosphere configuration, simulated using traditional MHD code with numerical

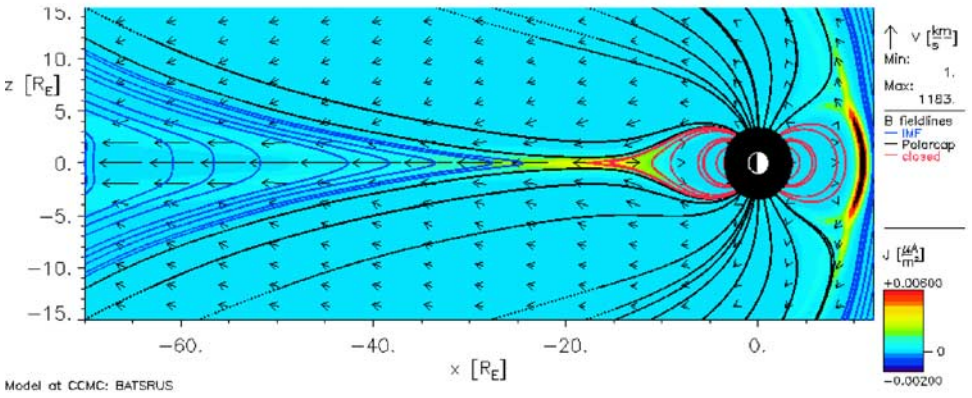

Figure 5. Steady magnetosphere configuration simulated using the MHD code with numerical resistivity only.

resistivity, does not change much during 4 hours of continuous southward driving (Figure 5). For simulations with kinetic corrections the motion of the reconnection site does not stop at $-20\ R_E$ but proceeds further down the tail. The tailward retreat slows down when the reconnection site reaches $-30 \div -25\ R_E$ and then continues to move tailward with an almost constant average speed of about 1 R_E/min $\sim$100 km/s. Soon after the reconnection site nearest to the Earth retreats tailward beyond $-70\ R_E$ a new near-Earth reconnection site is formed. The tailward retreat of the newly formed reconnection site follows the same scenario described above.

[41] Thus the simulations with nongyrotropic corrections demonstrate a dynamic, quasi-periodic, response of the magnetosphere to the steady southward driving conditions. A video sequence (Animation 1)[1] shows magnetotail loading/unloading cycle that repeats itself over and over again during 5 hours of simulations. Figure 6 shows the magnetosphere evolution during one of the similar loading/unloading cycles (between 6:05 and 7:05 time stamps). The six panels in Figure 6 correspond to selected frames from Animation 1. Here colors display current density distribution at the $Y = 0$ plane and arrows correspond to velocity vectors. Blue lines are IMF field lines with both ends open, red lines are closed field lines connecting northern and southern polar regions, and black lines are semiopen lobe field lines connecting polar regions to IMF. At the beginning and at the end of the selected cycle, Figures 6a and 6f illustrate stretched magnetotail with embedded thin current sheet minutes prior to near-Earth reconnection onset. In between these two stages of the cycle the magnetotail experiences dynamical evolution: reconnection onset and formation of small plasmoids trapped in the area of closed field lines (Figure 6b), fast magnetic reconnection of lobe filed lines accompanied by large plasmoid ejection (Figure 6c), further tailward retreat of reconnection site (Figures 6d and 6e), and formation of thin current sheet earthward of the distant-tail reconnection site (Figure 6f). The current sheet in the diffusion region between reconnecting lobe field lines exhibits a bifurcated structure (Figure 6, Animation 1).

[1]Animation is available in the HTML.

[42] Figure 7 shows time variations in the magnitude of the reconnection electric field $E^{\mathrm{REC}} = E_0^{\mathrm{ng}}$ (Figure 7a) and the length of the diffusion region $2d_x$ (Figure 7b) at the reconnection site closest to the Earth X_0 for $Y = 0$. Vertical dashed lines mark the occurrences of near-Earth reconnection onsets. Horizontal dashed lines represent the levels of the reconnection rate (Figure 7a) and the length of the diffusion region (Figure 7b) for quasi-steady reconnection in global simulations with numerical resistivity. Global MHD simulations with kinetic corrections demonstrate that magnetotail reconnection is inherently unsteady (Figure 7). The important features, which typically are not produced in traditional global MHD simulations, are time intervals of very fast magnetotail reconnection. The bursts of fast reconnection last only for a few minutes. During the bursts the length of the diffusion region is small, not exceeding 2 R_E. A sharp peak in the reconnection rate, a small length of the diffusion region, and a bifurcated current sheet described above are also characteristic features of fast kinetic reconnection observed in small-scale kinetic simulations of antiparallel reconnection [*Hesse et al.*, 1999]. After reaching the maximum value the reconnection rate undergoes a pronounced decrease accompanied by an increase in the length of the diffusion region. Large peaks in time profile of the reconnection rate are closely followed by smaller boosts. The small raise in the reconnection rate occurs during temporal slowdown of the tailward retreat of the reconnection site at around $-\ 30 \div -25\ R_E$. These results are in agreement with recent kinetic simulations of magnetic reconnection in relatively large geometries with open boundary conditions [*Daughton et al.*, 2006]. After the reconnection site resumes its tailward motion with almost constant speed at about 100 km/s, the reconnection rate continues gradual decrease accompanied by the gradual increase of the diffusion region length. When the reconnection site reaches the distant tail beyond $-70\ R_E$ the reconnection rate and the length of the diffusion region approach levels corresponding to quasi-steady reconnection in global simulations with numerical resistivity.

[43] An overall state of the magnetospere at each time step can be characterized by the value of the magnetic flux in the tail lobes Ψ, calculated by integration of magnetic flux over the polar cap. After a long period of northward IMF the polar cap is almost closed and the value of Ψ is

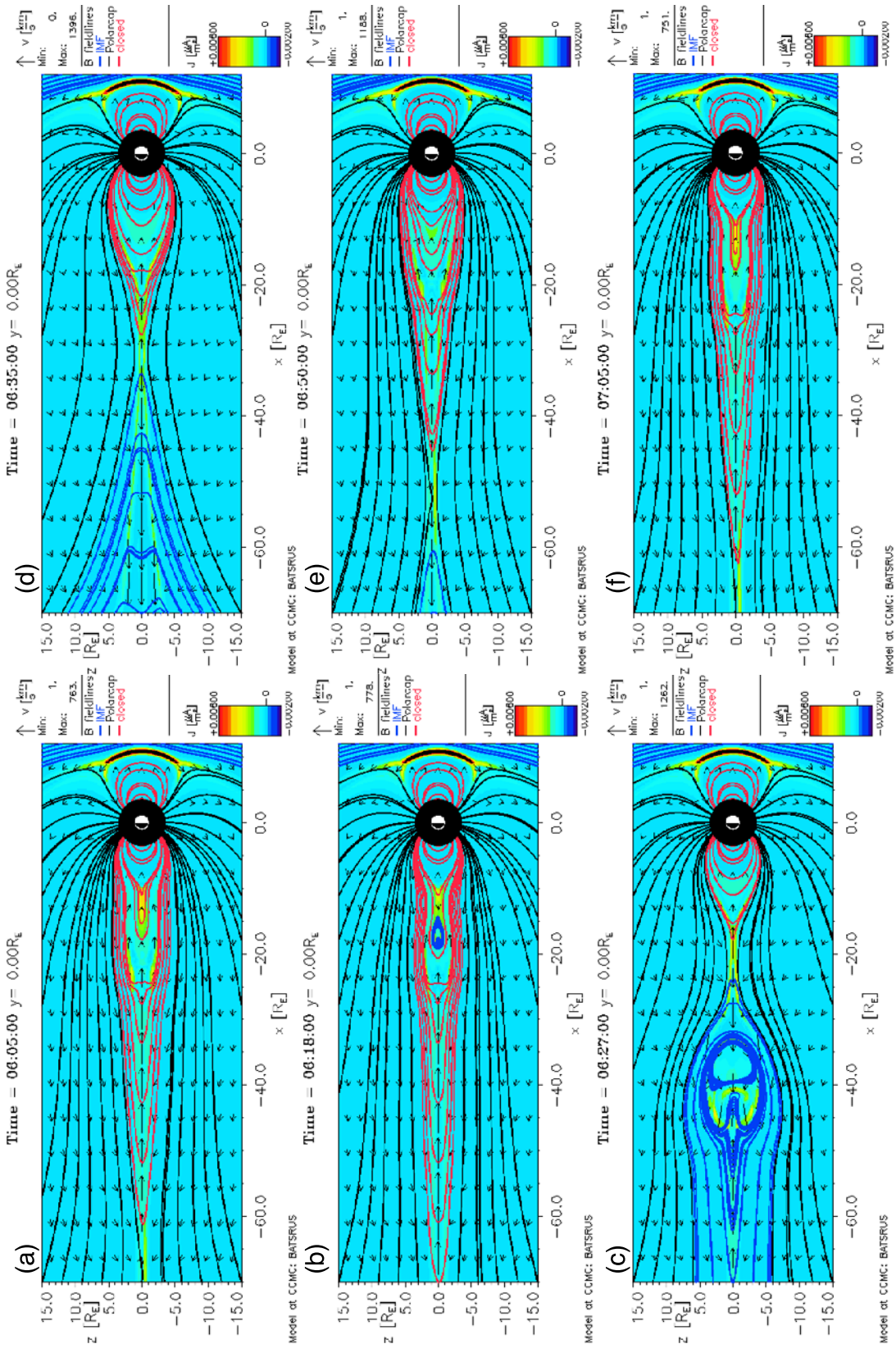

Figure 6. Overall magnetosphere evolution during one loading/unloading cycle (between 6:05 and 7:05). Color-coded current density distribution at $Y = 0$ plane. Arrows correspond to velocity vectors. Blue lines are interplanetary field lines with both open ends, red lines are closed field lines connecting northern and southern polar regions, and black lines are semiopen filed lines connections polar regions to IMF.

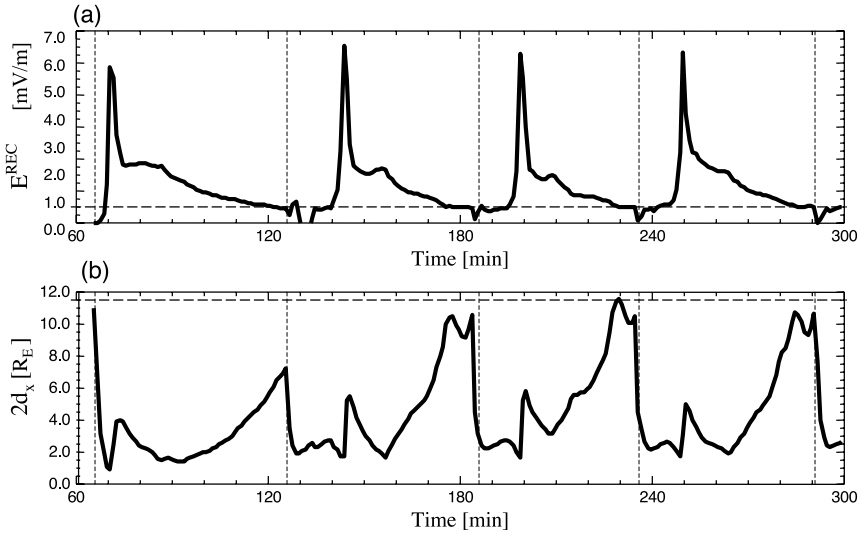

Figure 7. (a) The reconnection rate and (b) the length of the diffusion region at the closest to the Earth reconnection site X_0 for $Y = 0$. Vertical dashed lines show the time of the new near-Earth reconnection site formation. Horizontal lines show levels of reconnection rate and the length of the diffusion region for simulations with numerical resistivity. Time is measured in minutes past after the southward turning at time stamp 4:00.

very small. Dayside magnetic reconnection initiated after southward IMF turning at 4:00 time stamp provides steady magnetic flux loading into the tail lobes. Reconnection of lobe magnetic field lines in the magnetotail is responsible for the lobe magnetic flux unloading. In MHD simulations with numerical resistivity the loading and unloading of magnetic flux in magnetotail lobes neutralize each other after a few hours of southward driving, thus resulting in quasi-steady magnetosphere configuration shown in Figure 5. In MHD simulations with nongyrotropic corrections temporal variations of the open magnetic flux stored in the tail lobes Ψ (Figure 8) exhibit sawtooth-type oscillations with slow-loading ($\sim$1 hour) and fast-unloading ($\sim$5–10 min) phases. The fast-unloading phase is caused by bursts of magnetotail reconnection shown at Figure 7a. The amount of the magnetic flux released during each unloading phase is about 20% of average magnetic flux content in the lobe. Variations of magnetic flux shown at Figure 8 display characteristic features of multiple substorms.

[44] Periodic stretching and compression of the whole inner magnetosphere is illustrated in Figure 9. Here four time series represented by solid and dashed lines show magnetic field variations at four different virtual satellites at geosynchronous orbit (R = 6.6 R_E) between noon and midnight. Magnitudes of magnetic field oscillations range approximately from 5 nT at noon to 10 nT at midnight. Sawtooth signatures are especially pronounced at the nightside.

[45] Color-coded values of V_x component of bulk flow velocity in the equatorial plane $Z = 0$ at different stages of magnetotail reconnection are illustrated at Figure 10. Red and yellow areas at Figure 10 correspond to fast earthward flows from reconnection sites. Figure 10a shows the stretched magnetotail at the end of the loading phase 10 min prior to the second near-Earth magnetic reconnec-

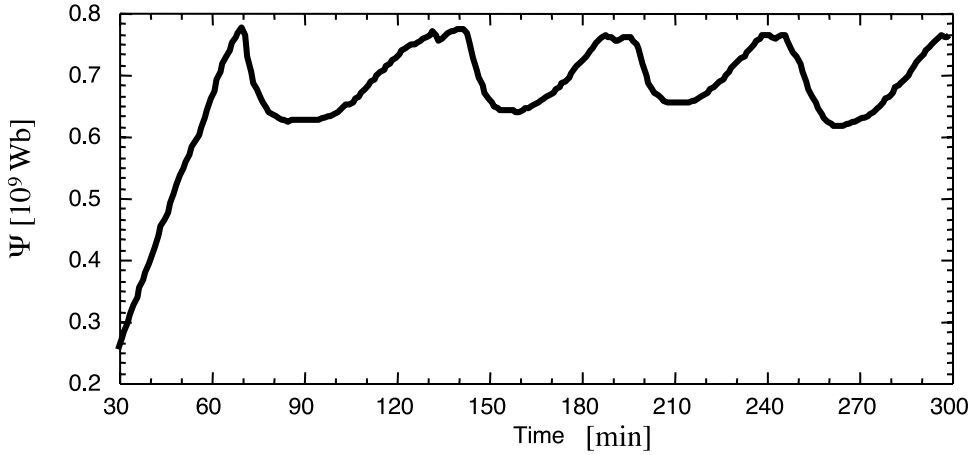

Figure 8. Open magnetic flux variations.

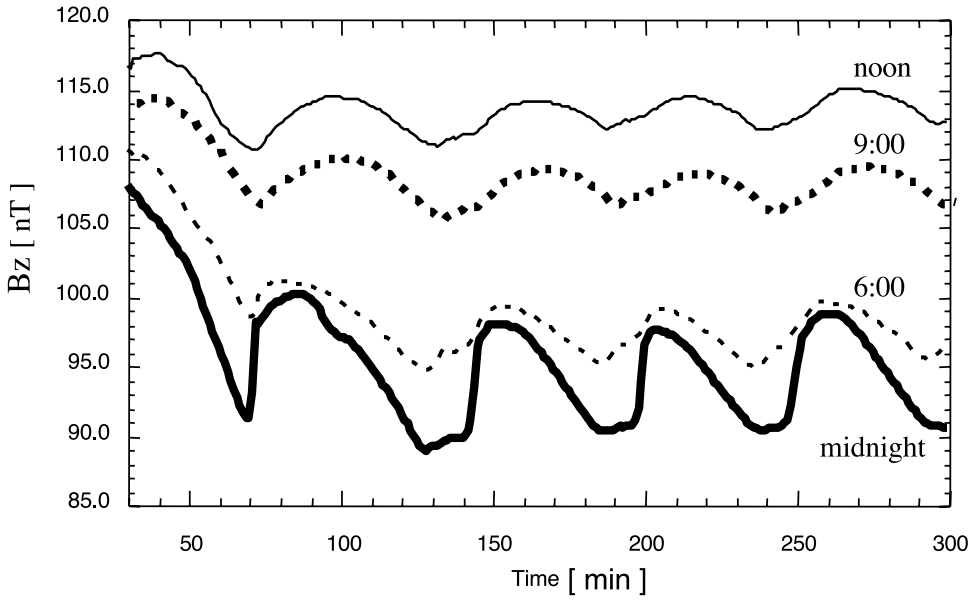

Figure 9. Magnetic field variations detected by virtual satellites at different locations along the geosynchronous orbit.

tion onset. Earthward plasma flows from the retreating reconnection site divert around the strong Earth's dipole magnetic field and interact with solar wind flows near the magnetopause, causing the wave-type distortion of the magnetopause boundary. Surface waves and vortices at the flanks during substorms can be observed by in situ measurements or detected by their signatures in the ionosphere. After the near-Earth reconnection onset the flow pattern in the equatorial plane exhibits narrow high speed velocity jets at the flanks (Figure 10b) accompanied by "broad-front" earthward and tailward flow bursts in the central plasma sheet (Figure 10c). Owing to continuous motion of reconnection site and subsequent reconfiguration of the flow pattern, virtual satellites in equatorial plane should detect unsteady bursty bulk flows.

[46] An example of virtual satellite observations of time profiles of V_x component of bulk flow velocity at magnetospheric flanks is shown in Figure 11. Virtual satellites are set at three different locations in equatorial plane $Z = 0$ along $X = 0$ line between the geosynchronous orbit and the magnetopause: $Y = 8\ R_E$ (dotted curve), $Y = 10\ R_E$ (thick solid curve), $Y = 12\ R_E$ (thin solid curve). Sunward flow bursts are detected at all three locations at the magnetospheric flanks. The velocity of sunward flow jets in region around $Y = 12\ R_E$ adjacent to the magnetopause reaches 400 km/s. Period of reoccurrence of high-speed jets is consistent with 1 hour time period of loading/unloading cycle. Superimposed 5-min-period oscillations, caused by Kelvin-Helmholtz surface waves, are most pronounced during the first loading stage after the southward IMF turning.

5. Summary and Conclusions

[47] The goal of this study is to develop and test a strategy of multiscale modeling of magnetic reconnection in global magnetosphere. In traditional global magnetosphere MHD simulations magnetic reconnection relies upon unphysical numerical dissipation or ad hoc anomalous resistivity. The new approach utilizes the results of kinetic analysis and incorporate the most essential kinetic effects in diffusion regions around the reconnection sites into global magnetospheric simulations. The key element of the approach is to identify diffusion regions where the gyrotropic fluid MHD approximation is not applicable. We developed an algorithm that searches for locations of magnetotail reconnection sites. The algorithm takes advantage of block-based domain-decomposition technique employed by BATS-R-US global MHD simulation code. Boundaries of the diffusion region around each reconnection site are estimated from the gyrotropic orbit threshold condition, where the ion gyroradius is equal to the distance to the reconnection site. Inside diffusion regions ions are treated as nongyrotropic fluid with nonzero off-diagonal components of the pressure tensor. The primary kinetic mechanism controlling the dissipation in the diffusion region is incorporated into global MHD simulations in terms of spatially localized nongyrotropic corrections to the induction equation [*Kuznetsova et al.*, 1998, 2000, 2001; *Hesse et al.*, 1999, 2001, 2004; Kuznetsova et al., submitted manuscript, 2007]. The magnitude of the nongyrotropic corrections to the electric field and spatial scales of the diffusion regions are calculated at each time step of the simulation using local MHD plasma and field parameters at the reconnection site without introduction of any ad hoc parameters.

[48] To clarify the role of nongyrotropic effects in diffusion region on the global magnetospheric dynamic we performed simulations for a long period of steady low-mach-number solar wind after IMF southward turning with parameters close to the average solar wind conditions during 18 April 2002 sawtooth event. The results of the simulations can be summarized as follows:

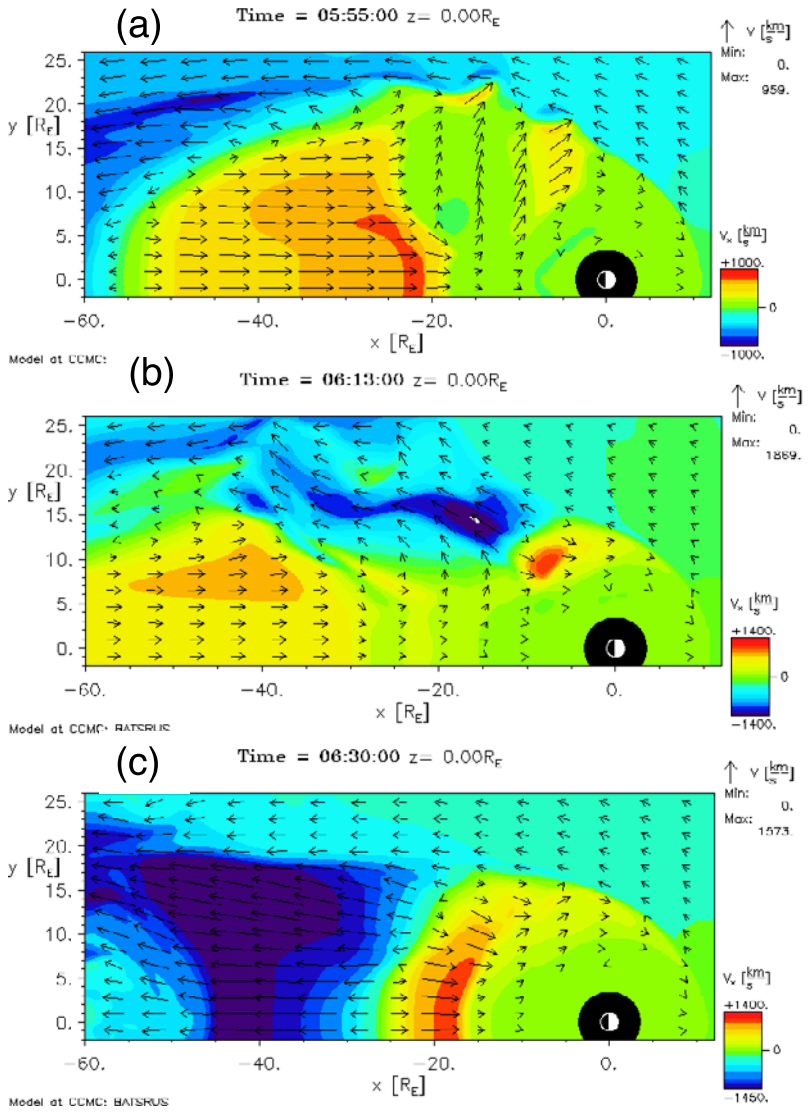

Figure 10. Bulk flow velocity patten at the equatorial plane.

[49] 1. Magnetotail reconnection is inherently unsteady even when the solar wind is steady.

[50] 2. Effects of nongyrotropic corrections become clearly evident in just a few minutes after the reconnection onset. Magnetic field and current density patterns in the vicinity of the reconnection site in global simulations with nongyrotropic corrections display many features characteristic of kinetic simulations of antiparallel magnetic reconnection, such as small length of the diffusion region, a bifurcated current sheet and a saddle-point in current density distribution at the reconnection site.

[51] 3. Global MHD simulations with nongyrotropic corrections produce bursts of fast reconnection typically observed in small-scale kinetic simulations. During the bursts the length of the diffusion region does not exceed $2R_E \sim 12\ c/\omega_{pi}$.

[52] 4. The bursts of the fast reconnection last only for a few minutes. After reaching the maximum value the reconnection rate decreases while the length of the diffusion region increases. The decreased rate, however, is still significantly larger that the steady reconnection rate characteristic for MHD simulations with reconnection supported by numerical resistivity alone.

[53] 5. Magnetotail reconnection supported by nongyrotropic effects results in a tailward retreat of the reconnection site with average speed of the order of 100 km/s, accompanied by magnetotail stretching and thin current sheet formation in the near-Earth plasma sheet.

[54] 6. Overall magnetosphere response to the steady southward IMF driving exhibits quasi-periodic loading/unloading dynamics typical for frequently observed multiple substorms. Each loading/unloading cycle is characterized by the following features: (1) bursts of fast reconnection, (2) tailward retreat of reconnection site, (3) current sheet thinning earthward of the retreating reconnection site followed by a new near-Earth reconnection site formation,

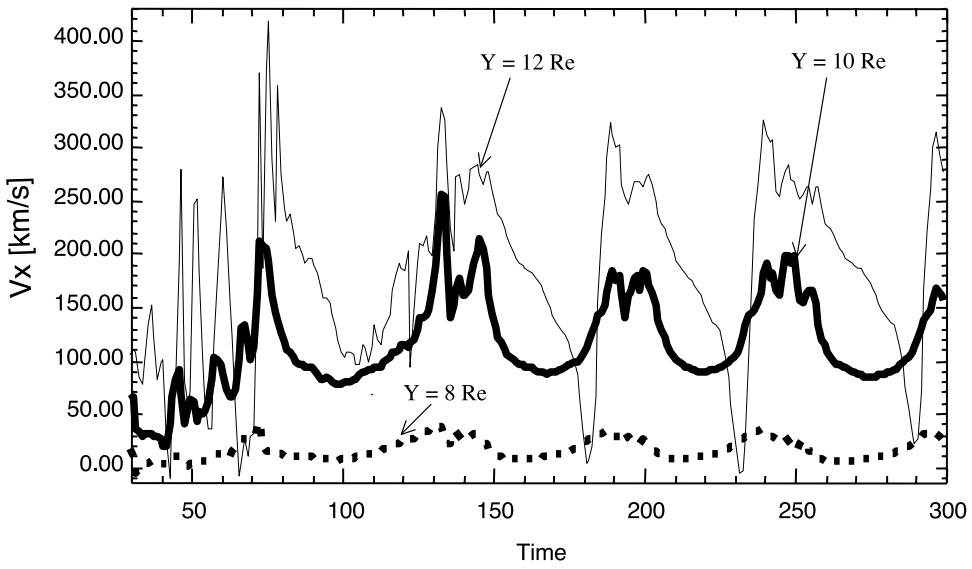

Figure 11. Sunward flow bursts at magnetospheric flanks at three different locations along $X = 0$, $Z = 0$ line between the geosynchronous orbit and the magnetopause: $Y = 8\ R_E$ (dotted curve), $Y = 10\ R_E$ (thick solid curve), $Y = 12\ R_E$ (thin solid curve).

(4) intermittent flow pattern in the equatorial plane, (5) sawtooth variations of open magnetic flux content in the tail lobes, (6) periodic stretching and compression of the dipole region in the inner magnetosphere, (7) sunward flow bursts at magnetospheric flanks, (8) generation of Kelvin-Helmholtz vortices at magnetospheric flanks during the loading phase.

[55] The consequences of this quasi-periodic magnetosphere behavior for inner magnetosphere ring current dynamics and resulting sawtooth oscillations of geosynchronous proton fluxes are discussed in the related paper by *Taktakishvili et al.* [2007].

[56] The simulated time period of loading/unloading cycle is about 2 times shorter than the mean timescale of observed sawtooth oscillations [*Borovsky et al.*, 1993; Borovsky et al., submitted manuscript, 2007]. This disagreement may be associated with a number of additional factors, not included in the present simulation with idealized symmetric settings. This issue will be addressed in the future work. To simulate real space weather events, the technique will be extended to asymmetric settings with finite B_y magnetic field component, nonzero dipole tilt, and realistic ionospheric conductance model.

[57] The key element of our approach is the search for reconnection sites. For simulations with symmetric modeled conditions used in this paper the search for the reconnection sites in the magnetotail is reduced to the search of B_x and B_z magnetic field reversals in the central plasma sheet close to the equatorial plane $|Y| < 18\ R_E$, $|Z| < 0.75\ R_E$. Preliminary results of simulations with finite IMF B_y, reported at AGU Fall Meeting 2006 [*Kuznetsova et al.*, 2006], showed that the search for reversal of two components in the plane perpendicular to the main current direction works well for IMF clock angles θ close to 180 degrees ($157° < \theta < 203°$). The search for reconnection sites for general nonsymmetric magnetotail will be refined in future publications. Possible solutions include utilizing methods of extracting the topological skeleton and critical point analysis [*Reitan et al.*, 2002; *Weinkauf et al.*, 2005]. The parallel magnetic field line tracing routine already implemented in the Space Weather Modeling Framework [*DeZeeuw et al.*, 2004; *Tóth et al.*, 2005] allows effective search for areas where differently connected field lines meet.

[58] The principal conclusion of this research is that the processes on kinetic scales strongly affect the global evolution of the magnetosphere. Therefore, an adequate description of non-MHD effects in diffusion regions is of critical importance for modeling of global magnetosphere dynamics, accurate identification of reconnection site locations, and prediction of possible spacecraft observations.

[59] Our approach allows one to include microphysics essential for the reconnection rate into large-scale models without posing large demands on computation efforts. We expect that global-scale MHD simulations with nongyrotropic corrections will lead to improved representations of space weather events in the magnetosphere.

[60] **Acknowledgments.** The authors appreciate stimulating discussions with Joe Borovsky, Jim Slavin, Janet Kozyra, and Mike Liemohn. G. T. has been partially supported by the Hungarian Science Foundation (OTKA, grant T047042). The simulations were performed at the Community Coordinated Modeling Center.

[61] Amitava Bhattacharjee thanks the reviewers for their assistance in evaluating this paper.

References

Amm, O. (1996), Comment on "A three-dimensional, iterative mapping procedure for the implementation of an ionosphere-magnetosphere anisotropic Ohm's law boundary condition in global magnetohydrodynamic simulations" by Michael L. Goodman, *Ann. Geophys.*, *14*, 773.

Ashour-Abdalla, M., M. El-Alaoui, V. Peroomian, R. J. Walker, L. M. Zelenyi, L. A. Frank, and W. R. Paterson (1999), Localized reconnection and substorm onset on Dec. 22, 1996, *Geophys. Res. Lett.*, *26*, 3545–3548.

Bessho, N., and A. Bhattacharjee (2005), Collisionless reconnection in an electron-positron plasma, *Phys. Rev. Lett.*, *95*, 245001, doi:10.1103/PhysRevLett.95.245001.

Birn, J., and M. Hesse (2001), Geospace Environment Modeling (GEM) magnetic reconnection challenge: Resistive tearing, anisotropic pressure and hall effects, *J. Geophys. Res.*, *106*, 3737–3750.

Birn, J., et al. (2001), Geospace Environment Modeling (GEM) magnetic reconnection challenge, *J. Geophys. Res.*, *106*, 3715–3720.

Birn, J., et al. (2005), Forced magnetic reconnection, *Geophys. Res. Lett.*, *32*, L06105, doi:10.1029/2004GL022058.

Borovsky, J. E. (2004), Global sawtooth oscillations of the magnetosphere, *Eos Trans. AGU*, *85*(47), Fall Meet. Suppl., Abstract SM23B-04.

Borovsky, J. E., R. J. Nemzek, and R. D. Belian (1993), The occurrence rate of magnetospheric-substorm onsets: Random and periodic substorms, *J. Geophys. Res.*, *98*, 3807–3814.

Borovsky, J. E., J. Birn, and A. J. Ridley (2004), BATSRUS/CCMC simulations of the magnetosphere for the solar-wind conditions that drive global sawtooth oscillations, *Eos Trans. AGU*, *85*(17), Jt. Assem. Suppl., Abstract SM12B-06.

Büchner, J., and A. Otto (1995), The influence of chaotic particle motion on large scale magnetotail stability, in *Space Plasmas: Coupling Between Small and Medium Scale Processes*, *Geophys. Monogr. Ser.*, vol. 86, edited by M. Ashour-Abdalla, T. Chang, and P. Dusenburg, pp. 197–204, AGU, Washington, D. C.

Büchner, J., and L. Zelenyi (1988), Reconnection instability in collisionless plasma, *Eur. Space Agency Spec. Publ.*, *ESA SP-285*, 21–28.

Daughton, W., J. Scudder, and H. Karimabadi (2006), Fully kinetic simulations of undriven magnetic reconnection with open boundary conditions, *Phys. Plasmas*, *13*, 072101, doi:10.1063/1.2218817.

DeZeeuw, D. L., S. Sazykin, R. A. Wolf, T. I. Gombosi, A. J. Ridley, and G. Tóth (2004), Coupling of a global MHD code and an inner magnetospheric model: Initial results, *J. Geophys. Res.*, *109*, A12219, doi:10.1029/2003JA010366.

Drake, J. F., M. Swisdak, C. Cattell, M. A. Shay, B. N. Rogers, and A. Zeiler (2003), Formation of electron holes and particle energization during magnetic reconnection, *Science*, *299*, 873–877.

Gombosi, T. I., G. Tóth, D. L. DeZeeuw, K. Hansen, K. Kabin, and K. Powell (2002), Semirelativistic magnetohydrodynamics and physics-based convergence acceleration, *J. Comput. Phys*, *177*, 176–205.

Gombosi, T. I., et al. (2004), Solution-adaptive magnetohydrodynamics for space plasmas: Sun-to-earth simulations, *Comput. Sci. Eng.*, *6*(2), 14–35.

Goodman, M. L. (1995), A three-dimensional, iterative mapping procedure for the implementation of an ionosphere-magnetosphere anisotropic Ohm's law boundary condition in global magnetohydrodynamic simulations, *Ann Geophys.*, *13*, 843–853.

Goodman, M. L. (1996), Reply to Olaf Amm's comment on "A three-dimensional, iterative mapping procedure for the implementation of an ionosphere-magnetosphere anisotropic Ohm's law boundary condition in global magnetohydrodynamic simulations" by Michael L. Goodman, *Ann. Geophys.*, *14*, 775.

Hesse, M. (2006), Dissipation in magnetic reconnection with guide magnetic field, *Phys. Plasmas*, *13*, 122107, doi:10.1063/1.2403784.

Hesse, M., and D. Winske (1998), Electron dissipation in collisionless *magnetic reconnection*, *J. Geophys. Res.*, *103*, 26,479–26,486.

Hesse, M., K. Schindler, J. Birn, and M. M. Kuznetsova (1999), The diffusion region in collisionless magnetic reconnection, *Phys. Plasmas*, *6*, 1781–1795.

Hesse, M., J. Birn, and M. M. Kuznetsova (2001), Collisionless magnetic reconnection: Electron processes and transport modeling, *J. Geophys. Res.*, *106*, 3721–3736.

Hesse, M., M. M. Kuznetsova, and J. Birn (2004), The role of electron heat flux in guide-field magnetic reconnection, *Phys. Plasmas*, *11*, 5387–5397.

Hesse, M., M. M. Kuznetsova, K. Schindler, and J. Birn (2005), Three-dimensional modeling of electron quasiviscous dissipation in guide-field magnetic reconnection, *Phys. Plasmas*, *12*, 100704, doi:10.1063/1.2114350.

Hoshino, M., K. Hirade, and T. Mukai (2001), Strong electron heating and non-Maxwellian behavior in magnetic reconnection, *Earth Planets Space*, *53*, 627–634.

Huang, C.-S., G. D. Reeves, G. Le, and K. Yumoto (2005), Are sawtooth oscillations of energetic plasma particle fluxes caused by periodic substorms or driven by solar wind pressure enhancements?, *J. Geophys. Res.*, *110*, A07207, doi:10.1029/2005JA011018.

Huba, J. D., N. T. Gladd, and K. Papadopoulos (1977), The lower-hybrid-drift instability as a source of anomalous resistivity for magnetic field line reconnection, *Geophys. Res. Lett.*, *4*, 125–128.

Karimabadi, H., D. Krauss-Varban, J. D. Huba, and H. X. Vu (2004), On magnetic reconnection regimes and associated three-dimensional asymmetries: Hybrid, Hall-less hybrid, and Hall-MHD simulations, *J. Geophys. Res.*, *109*, A09205, doi:10.1029/2004JA010478.

Kuznetsova, M. M., and B. Nikutowski (1994), A modified lower hybrid drift instability as a possible mechanism for generation of magnetic noise bursts in the magnetotail neutral sheet, *J. Geophys. Res.*, *99*, 4105–4114.

Kuznetsova, M. M., M. Hesse, and D. Winske (1998), Kinetic quasi-viscous and bulk flow inertia effects in collisionless magnetotail reconnection, *J. Geophys. Res.*, *103*, 199–214.

Kuznetsova, M. M., M. Hesse, and D. Winske (2000), Toward a transport model of collisionless magnetic reconnection, *J. Geophys. Res.*, *105*, 7601–7616.

Kuznetsova, M. M., M. Hesse, and D. Winske (2001), Collisionless reconnection supported by nongyrotropic pressure effects in hybrid and particle simulations, *J. Geophys. Res.*, *106*, 3799–3810.

Kuznetsova, M. M., M. Hesse, L. Rastätter, T. I. Gombosi, D. L. DeZeeuw, and G. Tóth (2006), Collisionless reconnection in global modeling of magnetospheric dynamics, *Eos Trans. AGU*, *87*(52), Fall Meet. Suppl., Abstract SM34B-03.

Otto, A. (2001), Geospace Environment Modeling (GEM) magnetic reconnection challenge: MHD and Hall-MHD—constant and current dependent resistivity models, *J. Geophys. Res.*, *106*, 3751–3758.

Powell, K. G., P. L. Roe, T. J. Linde, T. I. Gombosi, and D. L. DeZeeuw (1999), A solution-adaptive upwind scheme for ideal magnetohydrodynamics, *J. Comput. Phys.*, *154*, 284–309.

Pritchett, P. L. (2001a), Geospace Environment Modeling magnetic reconnection challenge: Simulations with a full particle electromagnetic code, *J. Geophys. Res.*, *106*, 3783–3798.

Pritchett, P. L. (2001b), Collisionless magnetic reconnection in a three-dimensional open system, *J. Geophys. Res.*, *106*, 25,961–25,978.

Pritchett, P. L. (2005), Onset and saturation of guide-field magnetic reconnection, *Phys. Plasmas*, *12*, 062301, doi:10.1063/1.1914309.

Pritchett, P. L., and F. V. Coroniti (2004), Three-dimensional collisionless magnetic reconnection in the presence of a guide field, *J. Geophys. Res.*, *109*, A01220, doi:10.1029/2003JA009999.

Raeder, J., R. L. McPherron, L. A. Frank, S. Kokubun, G. Lu, T. Mukai, W. R. Paterson, J. B. Sigwarth, H. J. Singer, and J. A. Slavin (2001), Global simulation of the Geospace Environment Modeling substorm challenge event, *J. Geophys. Res.*, *106*, 381–396.

Reitan, P., K. Keller, M. Kuznetsova, L. Rastätter, and M. Hesse (2002), Vector field visualization of magnetospheric dynamics, *Eos Trans. AGU*, *83*(19), Spring Meet. Suppl., Abstract SH52A-07.

Ricci, P., G. Lapenta, and J. U. Brackbill (2002), GEM reconnection challenge: Implicit kinetic simulations with the physical mass ratio, *Geophys. Res. Lett.*, *29*(23), 2088, doi:10.1029/2002GL015314.

Ricci, P., J. U. Brackbill, W. Daughton, and G. Lapenta (2004), Collisionless magnetic reconnection in the presence of a guide field, *Phys. Plasmas*, *11*, 4102–4114, doi:10.1063/1.1768552.

Ridley, A., T. Gombosi, and D. L. DeZeeuw (2004), Ionospheric control of the magnetosphere: Conductance, *Ann. Geophys.*, *22*, 567–584.

Rogers, B. N., R. E. Denton, J. F. Drake, and M. A. Shay (2001), Role of dispersive waves in collisionless magnetic reconnection, *Phys. Rev. Lett.*, *87*, 195,004.

Rogers, B. N., R. E. Denton, and J. F. Drake (2003), Signatures of collisionless magnetic reconnection, *J. Geophys. Res.*, *108*(A3), 1111, doi:10.1029/2002JA009699.

Shay, M. A., J. F. Drake, M. Swisdak, and B. N. Rogers (2004), The scaling of embedded collisionless reconnection, *Phys. Plasmas*, *11*, 2199–2213, doi:10.1063/1.1705650.

Slinker, S. P., J. A. Fedder, J. M. Ruohoniemi, and J. G. Lyon (2001), Global MHD simulation of the magnetosphere for November 24, 1996, *J. Geophys. Res.*, *106*, 361–380.

Sotnikov, V. I., V. D. Shapiro, and V. I. Shevchenko (1981), On the nonlinear theory of current instability of short-wave drift oscillations, *Physica D*, *20*, 170–184, doi:10.1016/0167-2789 (81)90071-3.

Soyka, J. J., R. Schunk, and M. Bowline (1997), Driving a physical ionosphere model with a magnetospheric MHD mode, *J. Geophys. Res.*, *102*, 22,209–22,220.

Taktakishvili, A., M. M. Kuznetsova, M. Hesse, M.-C. Fok, L. Rastätter, M. Maddox, A. Chulaki, T. I. Gombosi, and D. L. DeZeeuw (2007), Buildup of the ring current during periodic loading-unloading cycles in the magnetotail driven by steady southward interplanetary magnetic field, *J. Geophys. Res.*, *112*, A09203, doi:10.1029/2007JA012317.

Tóth, G., et al. (2005), Space Weather Modeling Framework: A new tool for the space science community, *J. Geophys. Res.*, *110*, A12226, doi:10.1029/2005JA011126.

Weinkauf, T., H. Theisel, K. Shi, H.-C. Hege, and H.-P. Seidel (2005), Extracting higher order critical points and topological simplification of 3D vector fields, in *Proceedings IEEE Visualization*, p. 71, IEEE, Minneapolis, Minn.

Wiltberger, M., T. I. Pulkkinen, J. G. Lyon, and C. C. Goodrich (2000), MHD simulation of magnetotail during the December 10, 1996, substorm, *J. Geophys. Res.*, *105*, 27,649–27,664.

Yin, L., and D. Winske (2003), Plasma pressure tensor effects on reconnection: Hybrid and Hall-magnetohydrodynamics simulations, *Phys. Plasmas*, *10*, 1595–1604, doi:10.1063/1.1559971.

Yin, L., D. Winske, S. P. Gary, and J. Birn (2001), Hybrid and Hall-MHD simulations of collisionless reconnection: Dynamics of the electron pressure tensor, *J. Geophys. Res.*, *106*, 10,761–10,776.

Zeiler, A., D. Biskamp, J. F. Drake, B. N. Rogers, M. A. Shay, and M. Scholer (2002), Three-dimensional particle simulations of collisionless magnetic reconnection, *J. Geophys. Res.*, *107*(A9), 1230, doi:10.1029/2001JA000287.

D. L. De Zeeuw, T. I. Gombosi, A. Ridley, and G. Toth, Center for Space Environment Modeling, University of Michigan, Ann Arbor, MI 48109–2143, USA.

M. Hesse, M. M. Kuznetsova, L. Rastätter, and A. Taktakishvili, Space Weather Laboratory, NASA Goddard Space Flight Center, Code 674, Bld. 21, Rm. 230, Greenbelt, MD 20771, USA. (maria.m.kuznetsova@nasa.gov)